Available online at www.sciencedirect.com
SCIENCE DIRECT
Journal of Molecular Catalysis A: Chemical 241 (2005) 184–193
JOURNAL OF MOLECULAR CATALYSIS A: CHEMICAL
www.elsevier.com/locate/molcata

Synthesis, characterization and evaluation of CeO_2/Mg,Al-mixed oxides as catalysts for SO_x removal

Carla Maria Salerno Polato [a], Cristiane Assumpção Henriques [b,*], Arnaldo Alcover Neto [c], José Luiz Fontes Monteiro [a]

[a] *NUCAT/COPPE/UFRJ, Caixa Postal 68502, CEP 21945-970, Rio de Janeiro, Brazil*
[b] *IQ/UERJ, Rua São Francisco Xavier, 524, CEP 20559-900, Rio de Janeiro, Brazil*
[c] *CETEM/MCT, Avenida Ipê 900, CEP 21941-590, Rio de Janeiro, Brazil*

Received 17 May 2005; received in revised form 28 June 2005; accepted 1 July 2005
Available online 19 August 2005

Abstract

Hydrotalcite-derived Mg,Al-mixed oxides (MO) with variable Mg/Al ratios (3, 1, 1/3) were impregnated with 17 wt.% of CeO_2 and evaluated for SO_x removal under conditions similar to those of FCC units. The catalyst with Mg/Al = 1, for which both an Mg(Al)O periclase-type and an $MgAl_2O_4$-spinel were present before sulfation, showed the best performance for both SO_x uptake and catalyst regeneration. The results from TPR/MS and XRD along reduction indicate the existence of different species in the sulfated samples. The reduction of these sulfate species leads to the evolution of SO_2 or H_2S, Mg(Al)O being the solid product in any case. Our results do not support the assertion that the reduction of S^{6+} to S^{2-} is a consecutive reaction. The evolution of SO_2 upon reduction decreases as the relative importance of the spinel-phase in the mixed oxides increases. The sulfates formed from the spinel-phase are more easily reduced than those from the periclase phase. The growth of the sulfate phase in the early stages of sulfation destroys the small mesopores of the mixed oxide. Upon regeneration, the sulfate phase is consumed and larger mesopores are formed.

Keywords: SO_x emission control; Sulfur-transfer catalysts; FCC unit; Mg,Al-mixed oxides; Mg,Al-spinels; Ceria; Hydrotalcites

1. Introduction

The burn-off of the sulfur-containing coke deposited on the catalyst in the regenerator of fluid catalytic cracking units results in SO_x (SO_2 and SO_3) emissions. Theses gases are among the major atmospheric pollutants and are acid rain precursors, posing a serious problem to the protection of the environment. In recent years, many refineries have taken measures to reduce SO_x emissions. One of those measures is the addition of SO_x transfer additives to the FCC catalyst. Those additives adsorb SO_x and so transfer sulfur back into the riser where it is released as H_2S, which is removed in the usual way (Claus process). This technique is very practical since the use of additives requires almost no capital investment, except for the cost of an additive loading system and the availability of a Claus plant. Three steps determine the performance of an SO_x transfer catalyst: (1) the oxidation of SO_2 to SO_3 under the FCC regenerator conditions, typically at 973–1003 K, (2) the trapping of SO_3 on the catalyst in the form of sulfates, and (3) the reduction of sulfates to release sulfur as H_2S in the FCC riser, typically at 793–803 K [1–5].

As to the composition of the SO_x transfer catalyst, basic oxides that form stable metal sulfates upon SO_3 adsorption would be the most efficient for the storage of SO_3. However, the stability of the sulfates should not be very high, since it can hinder the reduction step. Therefore, strong basic oxides, which form stable sulfates (MgO, CaO, BaO), are not suitable for this purpose. So, compounds of intermediate basicities such as $MgAl_2O_4$-spinel or Mg,Al-mixed oxides derived from hydrotalcite-like compounds (HTLCs) have attracted

* Corresponding author. Tel.: +55 21 2587 7322xR-46; fax: +55 21 25877227.
E-mail address: cah@uerj.br (C.A. Henriques).

1381-1169/$ – see front matter © 2005 Elsevier B.V. All rights reserved.
doi:10.1016/j.molcata.2005.07.006

much attention because they offer a large capacity of adsorption of SO_3, forming moderately stable metal sulfates under the conditions of the regenerator that can be decomposed in the reductive atmosphere of the cracking zone (riser). The presence of SO_x oxidation promoters as co-catalysts is also necessary since the SO_3 content in the regenerator is relatively low.

Hydrotalcites are layered double magnesium-aluminum hydroxides with general formula:
$[Mg_{8-x}Al_x(OH)_{16}(CO_3{}^{2-})_{x/2}]\cdot nH_2O$ $(0.20 \leq x \leq 0.33)$,
whose structure consists of brucite-like layers, where each Mg^{2+} ion is octahedrally surrounded by six OH^- ions and the different octahedra share edges to form infinite sheets. When Mg^{2+} cations are replaced isomorphously by Al^{3+}, the brucite-like layers become positively charged and the electrical neutrality is attained by the compensating carbonate anions located in the interlayers along with water molecules [6,7]. Thermal treatment of hydrotalcites at about 723–773 K induces dehydration, dehydroxilation and loss of compensation anions, forming Mg,Al-mixed oxides with a poor crystallized MgO-type structure, large specific surface area and basic properties. When the calcination is performed at about 1100 K or above, the formation of $MgAl_2O_4$-spinel-type phases was also observed [6,8]. These mixed oxides are widely used as active and selective catalysts in various basic-catalyzed reactions [9–12] and by incorporating transition metals (by coprecipitation or impregnation) redox properties are introduced. These characteristics, basicity and redox properties, which can be adjusted in order to achieve the optimal catalytic behavior, have allowed the development of new applications of mixed oxides derived from hydrotalcites as environmental catalysts, specially in the field of gas purification.

Literature reports that CeO_2 is widely used as oxidation promoter in SO_x removal catalysts. The role of ceria is derived from its basic/redox character. Ceria reducibility enhances the oxidation of SO_2 to SO_3 under FCC regeneration conditions by reacting with SO_2 to give substoichiometric cerium oxide, which is then reoxidized by oxygen. According to [13] its basic sites allow the adsorption of SO_2/SO_3 with formation of sulfates. In addition, it helps the desorption of sulfates as hydrogen sulfide under reductive conditions.

So, ceria-containing magnesium aluminate spinel of the type $CeO_2/MgAl_2O_4$ or ceria-containing Mg,Al-mixed oxides ($CeO_2/MgAlO_x$), both derived from HTLCs, are catalytic systems that meet all the criteria to be of interest for this reaction [3, 13–29]. Although these systems have been widely studied, there is a lack of information on the physico-chemical characteristics of the solids after steps 2 and 3, trapping of SO_x on the catalyst and the regeneration of the additive in the riser, respectively. So, in the present work, Mg,Al-mixed oxides with different Mg/Al ratios and impregnated with 17 wt.% of CeO_2 were first evaluated as additives for SO_x removal under conditions similar to those of a typical FCCU and then, aiming at a better understanding of the process, textural and structural analyses were carried out for each step that determine the performance of an SO_x transfer catalyst.

2. Experimental

2.1. Mg,Al-HTLC synthesis

Hydrotalcite samples were prepared by coprecipitating, at room temperature, an aqueous solution of magnesium and aluminum cations (solution A) with a highly basic carbonate solution (solution B). Solution A, containing $Mg(NO_3)_2\cdot 6H_2O$ and $Al(NO_3)_3\cdot 9H_2O$ dissolved in distilled water was 1.5 M in (Al + Mg) with variable Mg/Al molar ratios (3, 1 and 1/3). Solution B was prepared by dissolving appropriate amounts of Na_2CO_3 and NaOH in distilled water in order to obtain a $[CO_3{}^{2-}]$ equal to 1.0 M and a pH equal to 13 during the aging of the gel. In the synthesis procedure, solution A was slowly dropped (60 mL/h) under vigorous stirring to solution B placed in a 150 mL PTFE reactor. The gel formed was aged under constant pH (13) for 18 h at 333 K. The solid obtained was then filtered and washed with distilled water (363 K) until pH 7. The Mg,Al-hydrotalcites obtained were dried at 353 K overnight. Then they were calcined under dry air from room temperature to 1023 K, at 10 K/min, and kept at this temperature for 2 h. The Mg,Al-mixed oxides obtained were named MOX, where X is related to the Al/(Al + Mg) molar ratio.

A cerium nitrate solution was impregnated on the mixed oxides in a rotavapor at 333 K. The material was dried overnight at 393 K and than calcined at 1023 K for 2 h. The calcined samples were named Ce/MOX. The solids were crushed and sieved to the range 63–105 μm (−150 + 250 mesh Tyler).

2.2. Physico-chemical characterization

The chemical composition of the synthesized samples was determined by X-ray fluorescence using a Rigaku spectrometer. X-ray powder diffraction patterns were recorded in a Rigaku X-Ray Diffractometer equipped with a graphite monochromator using Cu Kα, 40 kV and 40 mA. The regeneration of the sulfated additives was followed by in situ X-ray diffraction analyses. For these studies the temperature was raised in steps of 25 K from 803 K until the complete regeneration was obtained. The samples were kept at each temperature for 10 min under 30%H_2/He before data acquisition. Thermal decomposition of the as-synthesized hydrotalcite samples was evaluated by thermogravimetric analysis (TGA) and derivative thermal analysis (DTA) performed on a Rigaku Thermobalance TAS 100, operating under dry air flow at 10 K/min heating rate up to 1273 K.

The textural characteristics, such as specific surface area (BET), external area (*t*-plot) and pore volume (BJH), were determined by N_2 adsorption–desorption at 77 K in a

Micromeritics ASAP 2000. The samples were previously outgassed at 473 K, overnight.

Scanning electron microscopy (SEM) analyses were carried out in an LEO S440 scanning electronic microscope, equipped with an energy dispersion spectroscopy (EDS) microanalysis system Link ISIS L300 with an SiLi Pentafet detector. The accelerating voltage applied was 20 kV. Each sample was placed in a metallic support and covered with a fine layer of carbon of approximately 30 nm in a BAL-TEC SCD 005 Sputter Coater.

2.3. Catalytic tests

During the SO_2 pick-up reaction, a stream of 175 mL/min with 1500 ppm of SO_2, 1.5% (v/v) O_2 and He balance was passed over 30 mg of the catalyst in a fixed bed micro-reactor at 973 K. The adsorption cycle was finished after a time on stream of 4 h. For catalyst regeneration (reduction step), the system was flushed with He and the sample was cooled down to 803 K. Then, He was shut off and the catalyst was reduced in a stream of 130 mL/min of H_2(30%)/He(70%) for 30 min, at 803 K. After that, the temperature was ramped to 1073 K at 5 K/min, under the same atmosphere. An additional test was done with sample Ce/MO50 in which the sulfated catalyst was reduced in a stream of 130 mL/min of C_3H_8(30%)/He(70%) under similar temperature conditions. The evolution of the products, in both steps, was followed by on line mass spectrometry using a Balzers quadrupole spectrometer (Model PRISMA-QMS 200). The release of SO_2 (m/z = 48 and 64), H_2S (m/z = 33 and 34), water (m/z = 18), hydrogen (m/z = 2) and oxygen (m/z = 16 and 32) was monitored.

3. Results and discussion

3.1. Physico-chemical characterization

3.1.1. Physico-chemical characteristics of the precursors

The results of chemical analysis of the HTLCs samples, expressed by their Al/(Al + Mg) molar ratio, are shown in Table 1. As can be observed these values are quite similar to those of the synthesis gel, indicating that the incorporation of both Mg and Al from the gel was nearly complete.

The X-ray diffractograms of the as-synthesized HTLC samples are shown in Fig. 1. Sample HT25 shows the characteristic pattern of pure hydrotalcite in carbonate form. For sample HT50, besides the hydrotalcite peaks, diffraction lines

Table 1
Chemical composition of HTLCs

Sample	$Al/(Al + Mg)_{gel}$	$Al/(Al + Mg)_{sample}$	Mg/Al
HT25	0.25	0.24	3
HT50	0.50	0.47	1
HT75	0.75	0.75	1/3

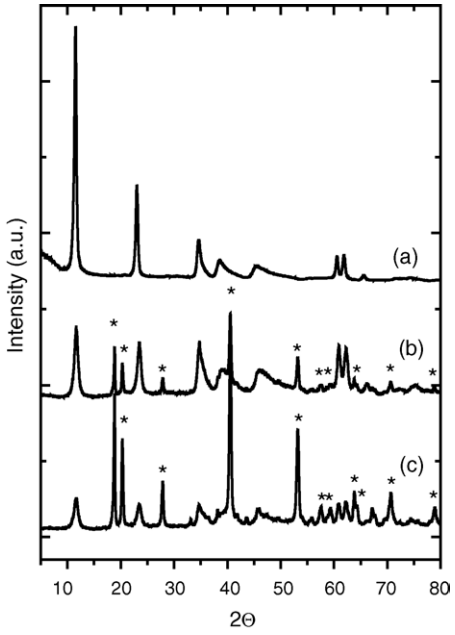

Fig. 1. Diffraction patterns of the as-synthesized precursors: (a) HT25, (b) HT50 and (c) HT75. (*) Bayerite phase—$Al(OH)_3$.

corresponding to a bayerite (aluminum hydroxide, $Al(OH)_3$) phase were observed, whereas for sample HT75 bayerite was the main phase formed. For Al/(Al + Mg) molar ratios greater than 0.33 the number of neighboring Al^{3+} ions in the hydroxide layers increases, so exceeding the repulsion among the positive charges that are responsible for keeping distant the Al^{3+} ions and leads to the generation of $Al(OH)_3$ [7].

For the pure hydrotalcite sample (HT25), the TGA/DTA results are in good agreement with those from the literature [7,30–32], which reports that hydrotalcites in the carbonate form present two well-defined weight losses. The first, up to 500 K, corresponds to the loss of interlayer water, and the second, between 548 and 723 K, is associated to dehydroxilation and decarbonation.

An intermediate loss was observed between 533 and 543 K for samples HT50 and HT75. It was associated to the dehydroxilation of the bayerite phase identified by XRD in both samples, which was confirmed by TGA/DTA of a sample of pure bayerite. The TGA results indicated that nearly 28 wt.% of sample HT50 corresponds to the bayerite phase whereas for sample HT75 this value is about 72 wt.%.

For all the calcined samples, XRD diffraction patterns (Fig. 2) of a poorly crystallized Mg(Al)O with a periclase-type structure were observed. In the case of the bayerite-containing samples, a γ-Al_2O_3-phase, associated to the thermal decomposition of the bayerite, was also formed.

Inspection of the N_2 adsorption/desorption results indicated that all samples presented IUPAC type IV isotherms, confirming that the thermal decomposition of the hydrotalcite samples at 1023 K produced mesoporous Mg,Al-mixed oxides. Their main textural characteristics are shown in Table 2. For sample MO25, the pores ranged between 100

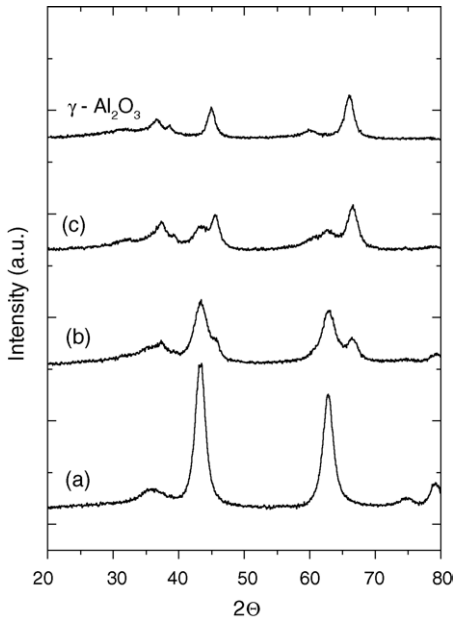

Fig. 2. X-ray spectra of the mixed oxides samples and of γ-alumina derived from bayerite calcined at 1023 K. (a) MO25; (b) MO50; (c) MO75.

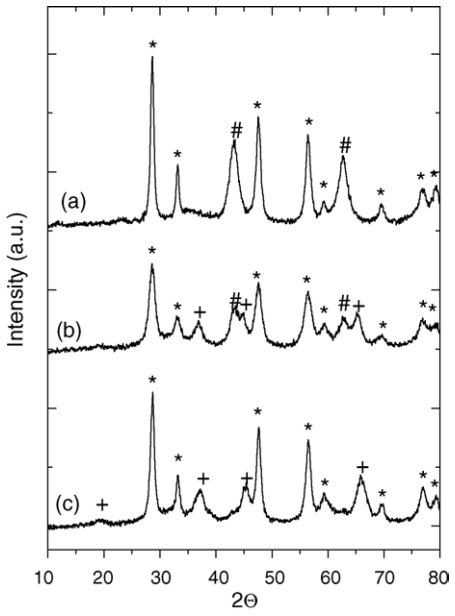

Fig. 3. X-ray diffraction patterns of the mixed oxides impregnated with cerium. (a) Ce/MO25; (b) Ce/MO50; (c) Ce/MO75. (*) CeO_2; (#) Mg(Al)O-periclase; (+) $MgAl_2O_4$.

and 900 Å, with a maximum at 500 Å. As the amount of aluminum increases, a second range of mesopores between 20 and 60 Å appears. Besides, the larger pores for both samples MO50 and MO75 range between 80 and 400 Å, with a maximum at about 150–200 Å. For sample MO75 a bimodal distribution can be clearly observed. From these observations, the smaller pores were associated to the alumina phase and the larger ones to the Mg(Al)O phase. The composition of this latter phase is expected to be roughly the same for samples MO50 and MO75, since their parent hydrotalcites, as indicated before, are not stable for Al/(Al + Mg) molar ratios greater than 0.33. This agrees with the pore size distribution of this phase being the same for samples MO50 and MO75. Furthermore, since samples MO50 and MO75 have roughly the same mesoporous volume, the specific surface area of the latter is larger as a consequence of the contribution of the smaller pores.

3.1.2. Cerium-containing samples

The X-ray diffractograms of the Ce-impregnated Mg,Al-mixed oxides are shown in Fig. 3. They show the diffraction pattern of the CeO_2 phase, which is marked with (*) in the figure. It can also be observed that the diffractograms are strongly influenced by the chemical composition of the mixed oxide. So, for the sample with the lowest aluminum content (Ce/MO25) the presence of the characteristic peaks of a poorly crystallized Mg(Al)O periclase-type phase was also observed. This was the only phase present in the Mg,Al-mixed oxide used as precursor. Upon increasing the aluminum content, the formation of the $MgAl_2O_4$-spinel-phase was detected. For sample Ce/MO50, both $MgAl_2O_4$-spinel and Mg(Al)O periclase phases coexist whereas for the sample with the highest aluminum content (Ce/MO75) only the spinel-phase was observed along with the ceria phase.

Table 2
Textural analysis of the Mg,Al-mixed oxides

Samples	S_{BET} (m^2/g)	$S_{External}$ (m^2/g)	V_{meso} (cm^3/g)[a]
MO25	213	213	0.747
MO50	177	177	0.447
MO75	243	243	0.453
γ-Al_2O_3	226	226	0.337

[a] Calculated by BJH method (adsorption branch).

Table 3 presents the main results of chemical composition and of textural and morphological characteristics of the calcined ceria-impregnated mixed oxides. For sample Ce/MO25, the pores ranged between 40 and 300 Å, with a maximum at about 100 Å. This indicates that the ceria particles partially blocked the large pores of sample MO25 and this caused a significant decrease of both the mesoporous volume and the specific area (Table 2). For sample Ce/MO50 the pores in the range between 80 and 400 Å, associated to the Mg(Al)O phase, were significantly blocked causing a small increase in the amount of pores in the range 20–60 Å. As a consequence, the decrease of the specific surface area was not as important as the decrease of the mesoporous volume. For sample Ce/MO75, the bimodal distribution was still present but a clear reduction of the amount of pores in both ranges was observed. This caused large reduction of both the mesoporous volume and the specific surface area. The crystallite size of the CeO_2 phase went also through a minimum for sample Ce/MO50. This can be tentatively associated to both the textural characteristics of the original mixed oxides and

Table 3
Chemical composition and textural characteristics of the samples impregnated with cerium

Samples	CeO_2 (wt.%)	Mg/Al	S_{BET} (m^2/g)	$S_{External}$ (m^2/g)[a]	V_{meso} (cm^3/g)[b]	V_{micro} (cm^3/g)[a]	CeO_2 Crystallite size (Å)
Ce/MO25	18	3	104	54	0.120	0.022	125
Ce/MO50	21	1	153	153	0.207	–	68
Ce/MO75	17	1/3	143	36	0.198	0.056	101

[a] Calculated by *t*-plot method.
[b] Calculated by BJH method (adsorption branch).

Table 4
SO_x pick-up efficiency

Sample	SO_2 uptake (μmol/g)	Theoretical[a] (μmol/g)	SO_x pick-up efficiency (%)
Ce/MO25	2332	15089	15
Ce/MO50	11174	9360	119
Ce/MO75	2909	4295	68

[a] Calculated based on the assumption that only Mg atoms are available for sulfur pick-up.

to the interaction of CeO_2 with the different phases formed upon calcination.

3.2. Catalytic tests

The performance of the catalysts for SO_2 pick-up is compared in Table 4. The results showed that the sample with the intermediate aluminum content (Ce/MO50) presented the highest SO_2 pick-up capacity and SO_2 removal efficiency. For all samples it was possible to observe that the maximum rate of SO_x pick-up took place in the first 5 min of reaction (Fig. 4), which is extremely interesting since the contact time inside the FCC regenerator is about 5 or 10 min, depending on its operation mode (partial or total combustion, respectively). The theoretical sulfur uptake levels were calculated based on the assumption that only Mg atoms in the mixed oxide are available for sulfur pick-up, forming sulfates. Aluminum was not included in this calculation because of the thermal instability of its sulfate ($Al_2(SO_4)_3$) under the conditions used. Ceria was not considered as a sulfur pick-up component since X-ray diffraction patterns of the sulfated samples did not show the presence of cerium sulfate.

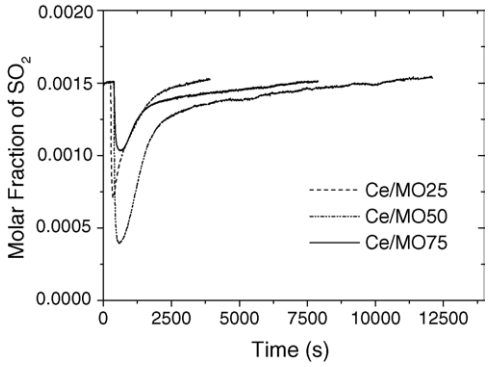

Fig. 4. SO_2 adsorption profile (T = 993 K, 1500 ppm SO_2, 1.5% (v/v) O_2 and He balance).

The calculated SO_x uptake efficiency showed that only 15% of the theoretical chemisorption sites in Ce/MO25 were utilized, while in Ce/MO75 this number corresponded to nearly 68% of the sites. It should be emphasized that the SO_x pick-up efficiency higher than 100% found for sample Ce/MO50 could indicate the possibility of the formation of other sulfate species. However, this hypothesis could not be confirmed by the X-ray diffraction analyses.

The SO_2 uptake capacity of the parent mixed oxides, MO25, MO50 and MO75, was 400, 381 and 369 μmol SO_2/g, respectively, much smaller than those of the corresponding ceria-containing samples (Table 4). So, the presence of an additional component with redox properties is fundamental for the use of the mixed oxides derived from hydrotalcites as a catalyst for SO_x removal.

XRD analyses of the Ce/MO25 sample before and after reaction showed the decrease of the periclase-type phase and the formation of $MgSO_4$ while the CeO_2 phase did not show any significant variation. Similar results were obtained for the Ce/MO50 sample, as can be seen in Fig. 5. In this case, the $MgAl_2O_4$-spinel was not significantly affected, suggesting that SO_3 is preferentially adsorbed on the Mg(Al)O phase. However, for sample Ce/MO75, for which the periclase-type phase was not originally present, the formation of $MgSO_4$

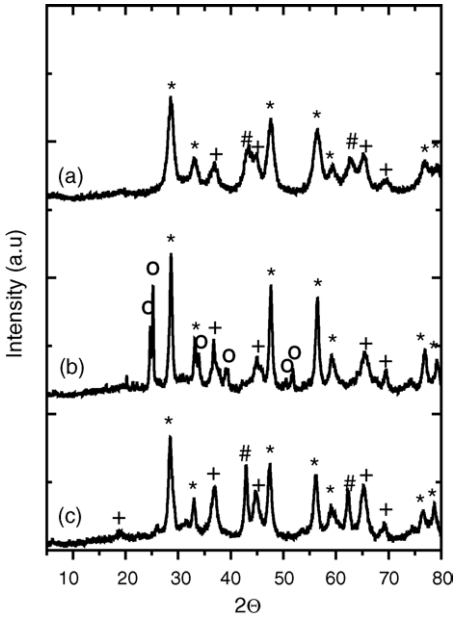

Fig. 5. Ce/MO50 sample. (a) Calcined; (b) sulfated; (c) regenerated. (*) CeO_2; (#) Mg(Al)O-periclase; (+) $MgAl_2O_4$; (◯) $MgSO_4$.

upon sulfation was observed, thus indicating the consumption of the spinel.

The results obtained from the TPR/MS runs showed that for all additives sulfur release started at temperatures higher than 803 K, the typical temperature found in the FCCU riser. Moreover, sulfur was released not only as H_2S but also as SO_2. In both cases, water was also liberated simultaneously.

For the sulfated Ce/MO25 sample (Fig. 6), TPR/MS studies indicated that H_2S release was preceded by the evolution of a significant amount of SO_2 (from about 850 K onwards). The onset temperature for H_2S release was about 920 K, substantially higher than that typical of the FCCU riser, and the presence of two distinct peaks at 945 and 1010 K could be observed. This behavior suggests the existence of different sulfate species, as proposed before by Waqif et al [33], and Wang and Li [34] based on IR studies. The presence of two peaks is also indicated by the SO_2 profile.

The results from in situ XRD analyses (Fig. 7) of this sample indicated that the transformation of magnesium sulfate into magnesium oxide can be clearly observed at 878 K, a temperature within the range where only SO_2 evolution was observed (with no H_2S release) in the TPR/MS analysis. These results indicated that in the case of sample Ce/MO25 at least one of the species formed upon sulfation is reduced into a periclase phase with the evolution of only SO_2. It should also be mentioned that no decomposition of the sulfate species was observed under inert atmosphere. Also, Fig. 7 shows that other magnesium sulfate species are still present at 928 K. We claim that such species are those which are reduced with the evolution of H_2S, as shown in Fig. 6. Since no other sulfur-containing solid phase was observed, the present results do not indicate that the reduction of S^{6+} to S^{2-} is a consecutive reaction, as proposed by Kim and Juskelis [19].

In the case of samples Ce/MO50 and Ce/MO75 (Figs. 8 and 9, respectively) SO_2 formation was much less important and simultaneous to H_2S release. Furthermore, it can be seen that SO_2 evolution decreases as the aluminum content or as the relative importance of the spinel-phase increase. So, it can be suggested that the sulfate species

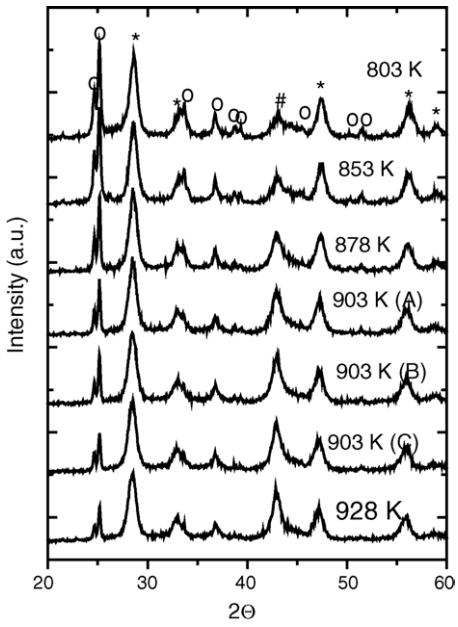

Fig. 7. In situ XRD analyses of the sulfated Ce/MO25 sample along reduction. Three data acquisitions were done at 903 K, with 30 min intervals between them. Phase identification as before.

which are reduced releasing SO_2 are formed from the periclase phase. This agrees with the largest evolution of SO_2 being observed for sample Ce/MO25.

As to the species that are reduced liberating H_2S, the present results demonstrate that they are formed from both the periclase and the spinel phases. The initial temperature for H_2S evolution decreased with increasing aluminum content, being about 878 and 842 K for Mg/Al molar ratios of 1 and 1/3, respectively. These results confirm that sulfates formed from the spinel-phase are more easily reduced than those from Mg(Al)O, as shown by Waqif et al. [33]. Although the two distinct peaks were present in all samples, the observed maxima shifted to lower temperatures and the relative importance of the second peak was higher the higher the aluminum content, again indicating the presence of different sulfate species, whether they originate from the periclase phase, from the

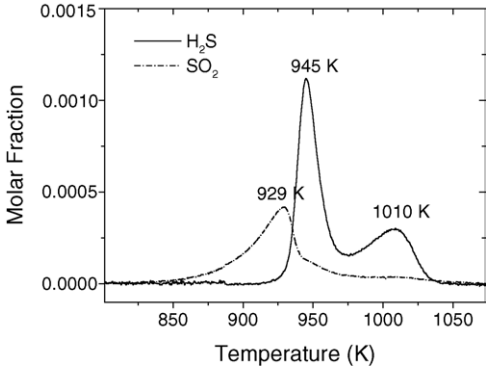

Fig. 6. Reduction profile for the sulfated Ce/MO25 sample (30%H_2/He for 30 min, at 803 K. After that, the temperature was ramped to 1073 K at 5 K/min).

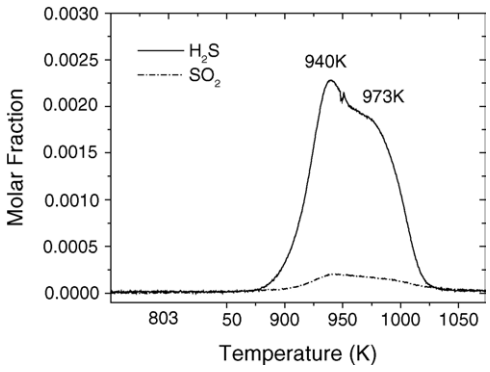

Fig. 8. Reduction profile for the sulfated Ce/MO50 sample (30%H_2/He for 30 min, at 803 K. After that, the temperature was ramped to 1073 K at 5 K/min).

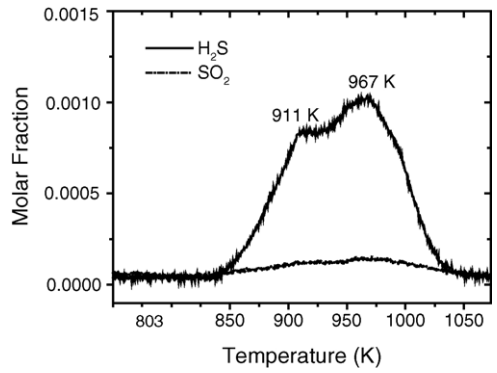

Fig. 9. Reduction profile for the sulfated Ce/MO75 sample (30%H_2/He for 30 min, at 803 K. After that, the temperature was ramped to 1073 K at 5 K/min).

spinel-phase or from both. Furthermore, the relative importance of the species which are more resistant to reduction is higher in the case of sulfates formed from the spinel-phase.

From the in situ XRD analyses (Figs. 10 and 11), the transformation of magnesium sulfate into magnesium oxide can be seen at 928 and 853 K for the sulfated Ce/MO50 and Ce/MO75 samples, respectively. Again these results are in agreement with those from TPR/MS. However, differently from what was observed for the sulfated Ce/MO25 sample, the phase transformations now observed derive from the reduction of magnesium sulfate, with H_2S evolution. Furthermore, the regeneration of the sulfated Ce/MO75 sample formed an Mg(Al)O-periclase-type phase, which was not present in the calcined sample before SO_2 oxidative adsorption. For the other two samples, the Mg(Al)O phase formed upon regeneration was already present before SO_x uptake.

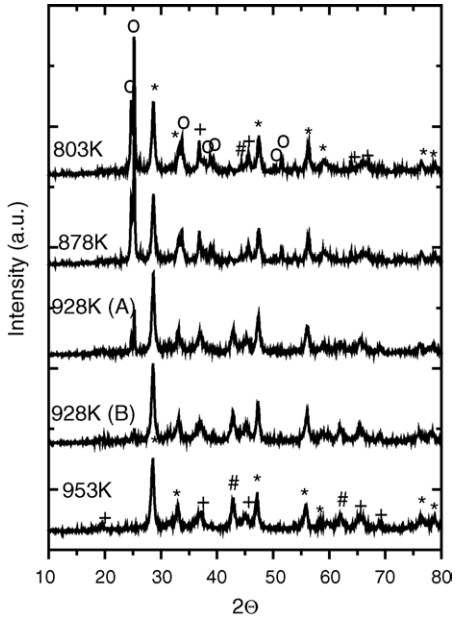

Fig. 10. In situ XRD analyses of the sulfated Ce/MO50 sample along reduction. Two data acquisitions were done at 928 K, with 30 min intervals between them. Phase identification as before.

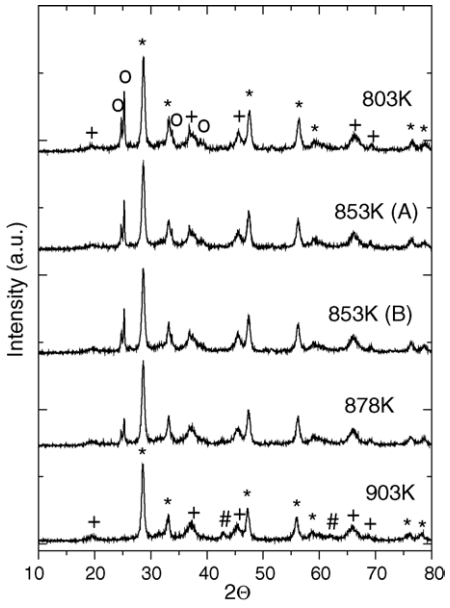

Fig. 11. In situ XRD analyses of the sulfated Ce/MO75 sample along reduction. Two data acquisitions were done at 853 K, with 30 min intervals between them. Phase identification as before.

Table 5 compares the amounts of H_2S and SO_2 released as well as the additive regeneration capacity defined as the ratio between the amount of SO_2 trapped on the catalyst and the amount of H_2S plus SO_2 released during the regeneration step. The best De-SO_x performance exhibited by Ce/MO50 among all the studied additives reflects the optimal balance between the basic properties responsible for SO_x pick-up efficiency, associated to Mg(Al)O-periclase phase, and the regeneration capacity related to the presence of the spinel-phase.

The regeneration step of the sulfated Ce/MO50 sample was also evaluated using propane (diluted in He) as reducing agent. Now, the regeneration was much poorer, with only 46% of the sulfur incorporated during the sulfation step (12348 μmol/g) being released. Furthermore, the amount of sulfur liberated as SO_2 (2199 μmol/g) was much higher than that when H_2 was used for reduction (Table 5). Although the liberation of H_2S (3447 μmol/g) took place roughly at the same temperatures as before, the same is not true for the evolution of SO_2, which now spans in a much larger temperature range. Both profiles also changed significantly, as can be seen in Fig. 12. Now, SO_2 was released in two clearly different temperatures, reinforcing the claim that two kinds of sulfate species are involved. The species corresponding to the second peak is clearly much more resistant to reduction

Table 5
Additive regeneration capacity

Sample	SO_2 (μmol/g)	H_2S (μmol/g)	Regeneration (%)
Ce/MO25	677	1132	78
Ce/MO50	1032	10096	100
Ce/MO75	324	2302	90

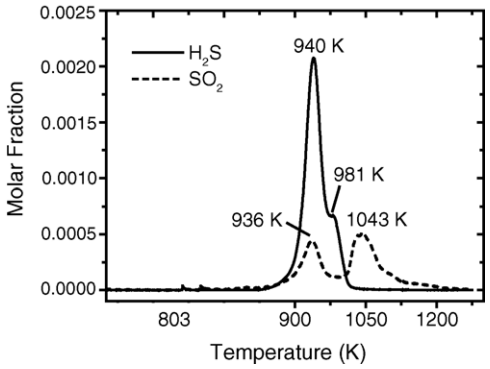

Fig. 12. Reduction profile for the sulfated Ce/MO50 sulfated sample (30%C_3H_8/He for 30 min, at 803 K. After that, the temperature was ramped to 1073 K at 5 K/min).

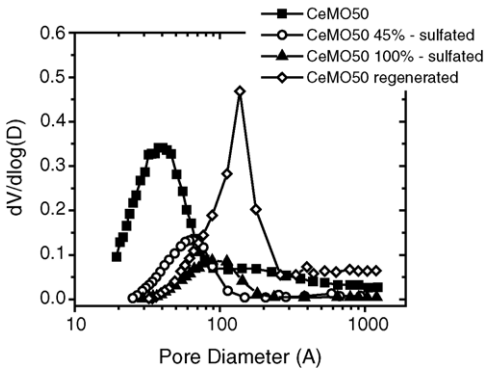

Fig. 13. Pore size distribution for sample Ce/MO50 before and after sulfation, and after regeneration.

by propane than by hydrogen. These findings do not support the reaction scheme proposed by Kim and Juskelis [19]. As to H_2S, the relative importance of the two peaks was significantly affected by the nature of the reducing agent, indicating that the corresponding sulfate species have different relative reactivities towards hydrogen and propane.

3.3. Textural characteristics of sample Ce/MO50 after the various steps

Taking into account its best performance as an additive for SO_x removal, the textural characteristics of sample Ce/MO50 were evaluated before and after each step, aiming at a better comprehension of the process.

Table 6 presents the results of textural analyses of the Ce/MO50 sample for different sulfating levels (45 and 100%) as well as for the regenerated sample. At 45% of its SO_x adsorption capacity, both BET specific surface area and mesoporous volume decreased markedly, indicating that the major part of the textural changes took place in the beginning of step 2 (trapping of SO_3 on the catalyst in the form of sulfates). This result can be confirmed by the adsorption profile of SO_2 (Fig. 4), where it is possible to observe that the maximum rate of SO_x pick-up took place in the first 5 min of reaction, quickly decreasing with time on stream. So, the differences in both the BET specific surface area and the mesoporous volume between the 100%-sulfated Ce/MO50 and the 45%-sulfated one are small. The regeneration of the former sample leads to a different pore volume distribution. For the calcined sample, pores ranged between 20 and 100 Å and for the regenerated sample between 50 and 250 Å, as shown in Fig. 13. As a consequence, the mesoporous volumes of both samples are similar, but the BET specific surface area of the regenerated sample is smaller. From the results in Table 6 and Fig. 13, we propose that the growth of the sulfate phase destroys the small mesopores present in sample Ce/MO50. The presence of this phase blocks the space available within the porous structure. Those two effects are responsible for

Table 6
Textural analyses of Ce/MO50 sample

Sample	S_{BET} (m^2/g)	$S_{External}$ (m^2/g)	V_{meso} (cm^3/g)
Ce/MO50	153	153	0.207
Ce/MO50 sulfated sample (45%)	30	24	0.058
Ce/MO50 sulfated sample (100%)	17	13	0.042
Ce/MO50 regenerated[a]	54	43	0.192

[a] Ce/MO50 100% sulfated and then regenerated under 30%H_2/He.

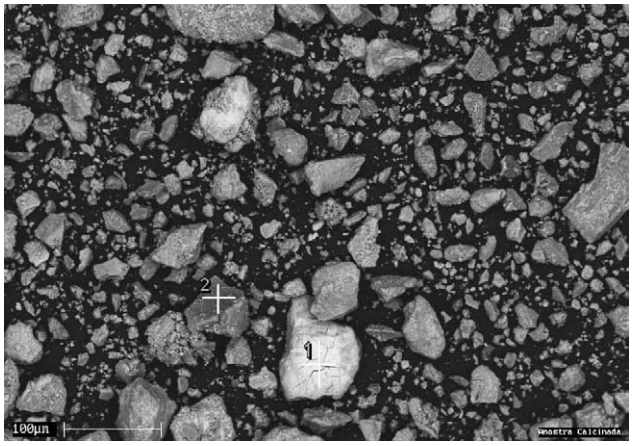

Fig. 14. Scanning electron microscopy of Ce/MO50 original sample.

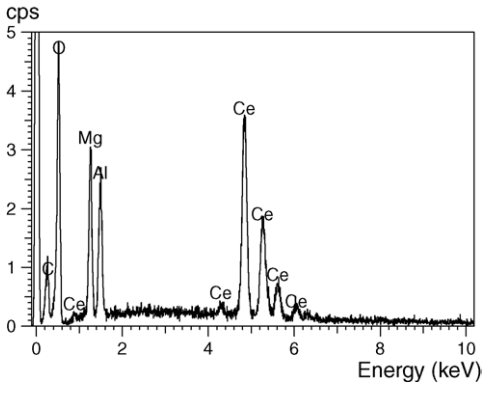

Fig. 15. EDS spectrum of region 1 in Fig. 14.

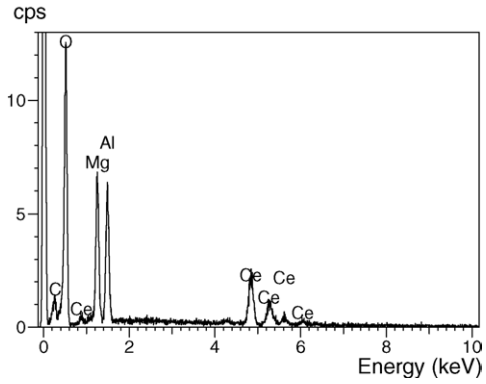

Fig. 16. EDS spectrum of region 2 in Fig. 14.

the small BET specific surface area and mesoporous volume observed for the sulfated samples. Upon regeneration, the sulfate phase disappears leaving behind larger mesopores.

SEM back scattered electron (BSE) images showed a heterogeneous distribution of both particle size and cerium concentration (as confirmed by EDS analyses) on the surface of the calcined mixed oxides (Figs. 14–16). The presence of the CeO_2 phase was indicated by the lighter regions in Fig. 14

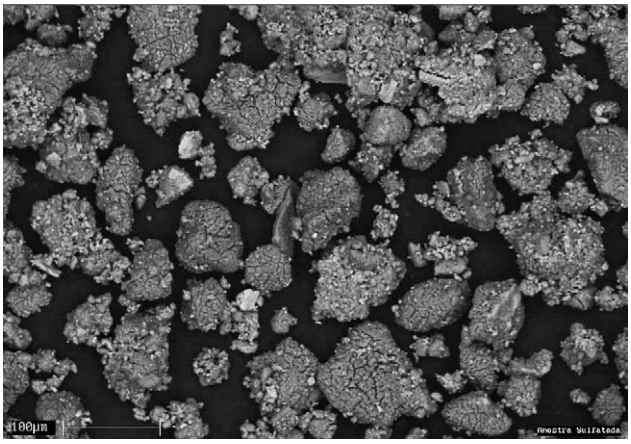

Fig. 17. Scanning electron microscopy of Ce/MO50 sulfated sample.

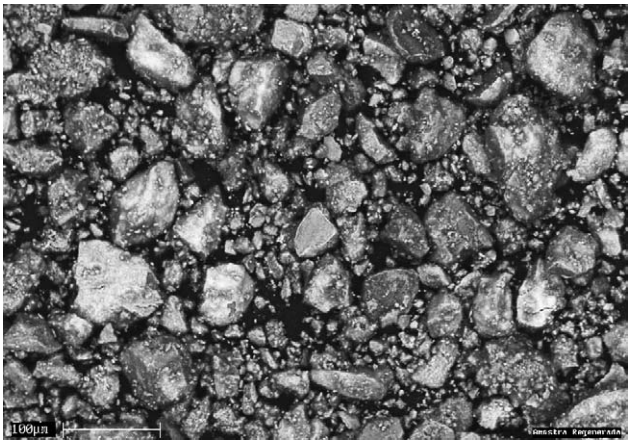

Fig. 18. Scanning electron microscopy of Ce/MO50 regenerated sample.

and was also confirmed by X-ray diffraction analyses. For the 100% sulfated sample, the results pointed out significant textural changes (Fig. 17), a sort of granulated surface being observed. This results from the growth of the sulfated phase on the external surface of the particles. Upon regeneration of the sulfated sample (Fig. 18), the original appearance is restored.

4. Conclusions

The results obtained in this work indicated that the mixed oxide with an Mg/Al molar ratio of 1, for which both periclase and spinel-phase were present, was the most effective as an SO_x transfer catalyst. The presence of different sulfate species was evidenced. These species were formed preferentially from the sulfation of Mg(Al)O but also from the sulfation of the $MgAl_2O_4$-spinel in the case of the sample with Mg/Al = 1/3, for which the spinel was the only phase present, besides ceria. The redox properties of ceria enhanced significantly the sulfur uptake capacity of the Mg,Al-mixed oxides, although no evidence for the formation of cerium sulfate could be observed. During the regeneration (reduction) step, sulfur was released to the gas phase both as SO_2 and H_2S, two peaks being observed for each of these gases along the TPR/MS run. This observation along with the results from XRD analysis of the sample along reduction indicate the presence of different sulfate species and do not support the assertion that the reduction of S^{6+} to S^{2-} is a consecutive reaction. On the contrary, our results indicate that some sulfate species are reduced with liberation of SO_2 while others with the direct evolution of H_2S, an Mg(Al)O periclase-type phase being the solid product in both cases whatever the composition of the original mixed oxide. The sulfate species which release SO_2 upon reduction are those formed from sulfation of the periclase phase originally present in the mixed oxides. Those which release H_2S upon reduction are formed from the sulfation of both the periclase and the spinel phases. So, the evolution of SO_2 decreases as the aluminum content or as the relative importance of the spinel-phase in the mixed oxides increase. The sulfates formed from the spinel-phase are more easily reduced than those from the periclase phase. As a consequence, the initial temperature for that evolution decreases as the aluminum content increases. The regeneration of the sulfated sample with propane was much less efficient than with H_2. Most of the textural changes of the solid took place in the early stages of sulfation when the growth of the sulfate phase destroys the small mesopores. Upon regeneration, the sulfate phase is consumed and larger mesopores are produced.

References

[1] W.C. Cheng, G. Kim, A.W. Peters, X. Zhao, K. Rajagopalan, Catal. Rev. Sci. Eng. 40 (1998) 39.

[2] A.E. Palomares, J.M. Lópes-Nieto, F.J. Lázaro, A. Lópes, A. Corma, Appl. Catal. B 20 (1999) 257.
[3] A. Corma, A.E. Palomares, F. Rey, Appl. Catal. B 4 (1994) 29.
[4] A. Corma, A.E. Palomares, F. Rey, F. Márques, J. Catal. 170 (1997) 140.
[5] J.A. Wang, L.F. Chen, R. Ballesteros, A. Montoya, J.M. Dominguez, J. Mol. Catal. A 194 (2003) 181.
[6] D. Tichit, M.H. Lhouty, G. Alain, B.H. Chiche, F. Figueras, A. Auroux, D. Bartalini, E. Garrone, J. Catal. 151 (1995) 50.
[7] F. Cavani, F. Triffirò, A. Vaccari, Catal. Today 11 (1991) 173.
[8] F. Rey, V. Fornés, J.M. Rojo, J. Chem. Soc., Faraday Trans. 83 (1992) 2233.
[9] A. Corma, V. Fornés, F. Rey, J. Catal. 148 (1994) 205.
[10] C. Noda Pérez, C.A. Pérez, C.A. Henriques, J.L.F. Monteiro, Appl. Catal. A 272 (2004) 229.
[11] M. Bolognini, F. Cavani, D. Scagliarini, C. Flego, C. Perego, M. Saba, Catal. Today 75 (2002) 103.
[12] M. Bolognini, F. Cavani, D. Scagliarini, C. Flego, C. Perego, M. Saba, Micropor. Mesopor. Mater. 66 (2003) 77.
[13] A. Trovarelli, C. Leitenburg, M. Borao, G. Dolcetti, Catal. Today 50 (1999) 353.
[14] J.A. Wang, L.F. Chen, C.L. Li, J. Mater. Sci. Lett. 17 (1998) 533.
[15] A.A. Bhattacharyya, G.M. Woltermann, J.S. Yoo, J.A. Karch, W.E. Cormier, Ind. Eng. Chem. Res. 27 (1988) 1356.
[16] S.J. Yoo, A.A. Bhattacharyya, C.A. Radlowiski, Appl. Catal. B 1 (1992) 169.
[17] J.C. Lavalley, M. Waqif, P. Bazin, O. Saur, G. Blanchard, O. Touret, Appl. Catal. B 11 (1997) 193.
[18] J.A. Wang, L.F. Chen, C.L. Li, J. Mol. Catal. A 139 (1999) 315.
[19] G. Kim, M.V. Juskelis, Stud. Surf. Sci. Catal. 101 (1996) 137.
[20] J.S. Yoo, J.A. Jaecker, US Patent 4,469,589 (1984).
[21] A.A. Chin, I.D. Johnson, C.T. Kresge, M.S. Sarli, US Patent 4,889,615 (1989).
[22] G. Kim, US Patent 5,288,675 (1994).
[23] J.S. Buchanan, M.F. Mathias, J.F. Sodomin, III, G.J. Teitman, US Patent 5,547,648 (1996).
[24] A. Bhattacharyya, M.J. Foral, W.J. Reagan, US Patent 5,750,020 (1998).
[25] E.W. Albers, H.W. Burkhead, Jr., US Patent 5,928,496 (1999).
[26] E.W. Albers, H.W. Burkhead, Jr., US Patent 6,156,696 (2000).
[27] E.J. Demmel, A.A. Vierheilig, R.B. Lippert, US Patent 6,281,164 (2001).
[28] W. Strehlau, U. Gobel, R. Domesle, E. Lox, T. Kreuzer, US Patent 6,338,831 (2002).
[29] A.A. Vierheilig, US Patent 6,479,421 (2002).
[30] A. Vacari, Appl. Clay Sci. 14 (1999) 161.
[31] T. Hibino, Y. Ymashita, K. Kosuge, A. Tsunashima, Clays Clay Miner. 43 (1995) 427.
[32] M. Bellotto, B. Rebours, O. Clause, J. Lynch, D. Bazin, E. Elkaim, J. Phys. Chem. 100 (1996) 8535.
[33] M. Waqif, O. Saur, J.C. Lavelley, Y. Wang, B.A. Morrow, Appl. Catal. 71 (1991) 319.
[34] J. Wang, C. Li, Appl. Surf. Sci. 161 (2000) 406.